

Geophysical Research Letters

RESEARCH LETTER

10.1029/2020GL089074

Key Points:

- Equilibrium warming per CO₂ doubling increases with CO₂ level for 13 of 14 climate models
- Positive feedback temperature dependence explains most of the sensitivity increase
- Nonlinear feedbacks increase the long-term risk of extreme warming under high CO₂ emissions

Supporting Information:

- Supporting Information S1

Correspondence to:

J. Bloch-Johnson,
j.bloch-johnson@reading.ac.uk

Citation:

Bloch-Johnson, J., Rugenstein, M., Stolpe, M. B., Rohrschneider, T., Zheng, Y., & Gregory, J. M. (2021). Climate sensitivity increases under higher CO₂ levels due to feedback temperature dependence. *Geophysical Research Letters*, 48, e2020GL089074. <https://doi.org/10.1029/2020GL089074>

Received 29 MAY 2020

Accepted 10 DEC 2020

Climate Sensitivity Increases Under Higher CO₂ Levels Due to Feedback Temperature Dependence

Jonah Bloch-Johnson¹ , Maria Rugenstein^{2,3} , Martin B. Stolpe³, Tim Rohrschneider², Yiyu Zheng² , and Jonathan M. Gregory^{1,4} 

¹NCAS, University of Reading, Reading, UK, ²Max Planck Institute for Meteorology, Hamburg, Germany, ³Department of Atmospheric Science, Colorado State University, Fort Collins, CO, USA, ⁴Met Office Hadley Centre, Exeter, UK

Abstract Equilibrium climate sensitivity—the equilibrium warming per CO₂ doubling—increases with CO₂ concentration for 13 of 14 coupled general circulation models for 0.5–8 times the preindustrial concentration. In particular, the abrupt 4 × CO₂ equilibrium warming is more than twice the 2 × CO₂ warming. We identify three potential causes: nonlogarithmic forcing, feedback CO₂ dependence, and feedback temperature dependence. Feedback temperature dependence explains at least half of the sensitivity increase, while feedback CO₂ dependence explains a smaller share, and nonlogarithmic forcing decreases sensitivity in as many models as it increases it. Feedback temperature dependence is positive for 10 out of 14 models, primarily due to the longwave clear-sky feedback, while cloud feedbacks drive particularly large sensitivity increases. Feedback temperature dependence increases the risk of extreme or runaway warming, and is estimated to cause six models to warm at least an additional 3K under 8 × CO₂.

Plain Language Summary Increasing CO₂ reduces the rate at which energy leaves Earth, causing a net energy gain at its surface. The resulting warming increases the rate that energy leaves the planet. The planet stops warming once it regains balance. Studies usually assume that doubling atmospheric CO₂ always produces the same eventual global temperature rise (called the “equilibrium climate sensitivity”), whatever the starting CO₂ level. We show, on the contrary, that in nearly all the computer climate models we have examined, the extra warming for each doubling goes up as the CO₂ level increases. In most models, the warmer the climate becomes, the more it has to warm in order to balance a further CO₂ doubling because warming becomes less effective at rebalancing the flow of energy. This effect increases projections of warming, especially for scenarios of greatest CO₂ increase.

1. Introduction

The *equilibrium climate sensitivity* (ΔT_{2x}) is the equilibrium global-mean surface warming per CO₂ doubling (Hansen et al., 1985; Stocker et al., 2013). ΔT_{2x} is often assumed to be constant (Stocker et al., 2013), allowing the equilibrium warming from different CO₂ increases to be characterized by a single metric and for time series with various CO₂ changes to be used to estimate ΔT_{2x} . A constant ΔT_{2x} rests on two assumptions: each CO₂ doubling induces the same radiative forcing, and each unit of forcing induces the same equilibrium warming (i.e., that the net radiative feedback is constant). However, for low or high enough CO₂ concentrations, the net radiative feedback becomes positive, causing runaway glaciation (Hoffman et al., 1998) or a runaway greenhouse (Ingersoll, 1969; Komabayasi, 1967), respectively. Given these limits, will ΔT_{2x} remain constant across the range of CO₂ levels expected under future emissions scenarios?

Paleoclimatologists have investigated this question (Farnsworth et al., 2019; Heydt et al., 2016). Studies of the early Cenozoic find an increase in climate sensitivity with CO₂ concentration (Anagnostou et al., 2016, 2020; Caballero & Huber, 2013; Farnsworth et al., 2019; Shaffer et al., 2016; Zhu et al., 2019), while studies of the Pleistocene disagree about whether sensitivity increases (three of four models in Crucifix, 2006; Friedrich et al., 2016; Köhler et al., 2017; Snyder, 2019; Yoshimori et al., 2009), stays the same (Martínez-Boti et al., 2015), or decreases (one of four models in Crucifix, 2006) with CO₂. However, different continental configurations may affect how sensitivity changes with CO₂ (Caballero & Huber, 2013; Farnsworth et al., 2019; Wolf et al., 2018).

While most studies of general circulation models under modern conditions have found that sensitivity increases with CO₂ (Bitz et al., 2012; Block & Mauritsen, 2013; Caballero & Huber, 2013; Duan et al., 2019;

Gregory et al., 2015; Hansen et al., 2005; Jonko et al., 2013; Meraner et al., 2013; Rieger et al., 2017; Rohrschneider et al., 2019), some have found that it decreases (Kutzbach et al., 2013; Stouffer & Manabe, 2003) or remains roughly constant (Colman & McAvaney, 2009). However, these 13 studies only evaluate ΔT_{2x} for models from five modeling centers. In most cases, they use mixed-layer oceans, neglecting changes in ocean dynamics that can affect sensitivity (Farnsworth et al., 2019; Kutzbach et al., 2013).

Recently, two datasets have become available with coupled atmosphere-ocean general circulation model (AOGCM) simulations at multiple constant CO₂ levels initialized under preindustrial conditions (abrupt $n \times \text{CO}_2$ simulations, where $n \times \text{CO}_2$ refers to the increase relative to preindustrial CO₂ concentration): 10 Coupled Model Intercomparison Project Phase 6 (CMIP6) models with abrupt 0.5 $\times \text{CO}_2$ and abrupt 2 $\times \text{CO}_2$ simulations run as part of NonLinMIP (Good et al., 2016) in addition to the standard abrupt 4 $\times \text{CO}_2$ simulations (Eyring et al., 2016), and five models in the LongRunMIP archive (a collection of 1,000+ year simulations of coupled AOGCMs; Rugenstein et al., 2019) with abrupt 2 $\times \text{CO}_2$, abrupt 4 $\times \text{CO}_2$, and abrupt 8 $\times \text{CO}_2$ simulations. One model participated in both projects.

In this paper, we show that equilibrium climate sensitivity generally increases with CO₂ level (Section 2); that changes in radiative forcing are not large enough to explain this increase for most models (Section 3); and that the increase is instead caused by positive feedback temperature dependence, with some contribution from feedback CO₂ dependence (Section 4). We compare these three nonlinear terms and their causes (Section 5) and then summarize our findings (Section 6).

2. Equilibrium Warming

Let T be the globally averaged surface temperature and $\Delta T \equiv T - T_{pi}$ be the warming relative to the preindustrial period. We define $\Delta T_{eq}(C)$ as the equilibrium warming caused by changing the CO₂ concentration from its preindustrial value ($p\text{CO}_{2,pi} \approx 280\text{ppm}$) to a new value ($p\text{CO}_2$), where C is the number of CO₂ doublings relative to this preindustrial period,

$$C(p\text{CO}_2) \equiv \log_2 \left(\frac{p\text{CO}_2}{p\text{CO}_{2,pi}} \right) \quad (1)$$

Under preindustrial conditions, $C_{pi} = 0$; in an abrupt 2 $\times \text{CO}_2$ simulation, $C = 1$; and so forth. Table S1 is a glossary of all symbols used in this paper.

One condition for equilibrium is that the net top-of-atmosphere radiative flux N (downwards positive) is zero, on average. If we assume that N depends solely on C and T , then we can express a change in N in an abrupt $n \times \text{CO}_2$ simulation as an initial change due to C and a subsequent change due to T :

$$N(C, T) - N(C_{pi}, T_{pi}) = \left(N(C, T_{pi}) - N(C_{pi}, T_{pi}) \right) + \left(N(C, T) - N(C, T_{pi}) \right) \quad (2)$$

$$N(C, T) - N(C_{pi}, T_{pi}) = \left(N(C, T_{pi}) - N(C_{pi}, T_{pi}) \right) + \int_{T_{pi}}^{T_{pi} + \Delta T} \frac{\partial N(C, T)}{\partial T} dT \quad (3)$$

$$N(C, T) - N(C_{pi}, T_{pi}) = F(C_{pi}, T_{pi}, C) + \int_{T_{pi}}^{T_{pi} + \Delta T} \lambda(C, T) dT \quad (4)$$

F is the *radiative forcing*, the change in N relative to a given initial condition (C_i, T_i) caused by C doublings of CO₂ while holding surface temperature fixed ($F(C_i, T_i, C) \equiv N(C_i + C, T_i) - N(C_i, T_i)$), and λ is the *radiative feedback*, the dependence of N on T ($\lambda(C, T) \equiv \partial N(C, T) / \partial T$), where the sign convention implies the feedback is typically negative. We can find $\Delta T_{eq}(C)$ by setting $N(C, T) = 0$:

$$F(C_{pi}, T_{pi}, C) = - \int_{T_{pi}}^{T_{pi} + \Delta T_{eq}(C)} \lambda(C, T) dT \quad (5)$$

where we assume $N(C_{pi}, T_{pi}) = 0$, since the preindustrial climate was roughly in equilibrium.

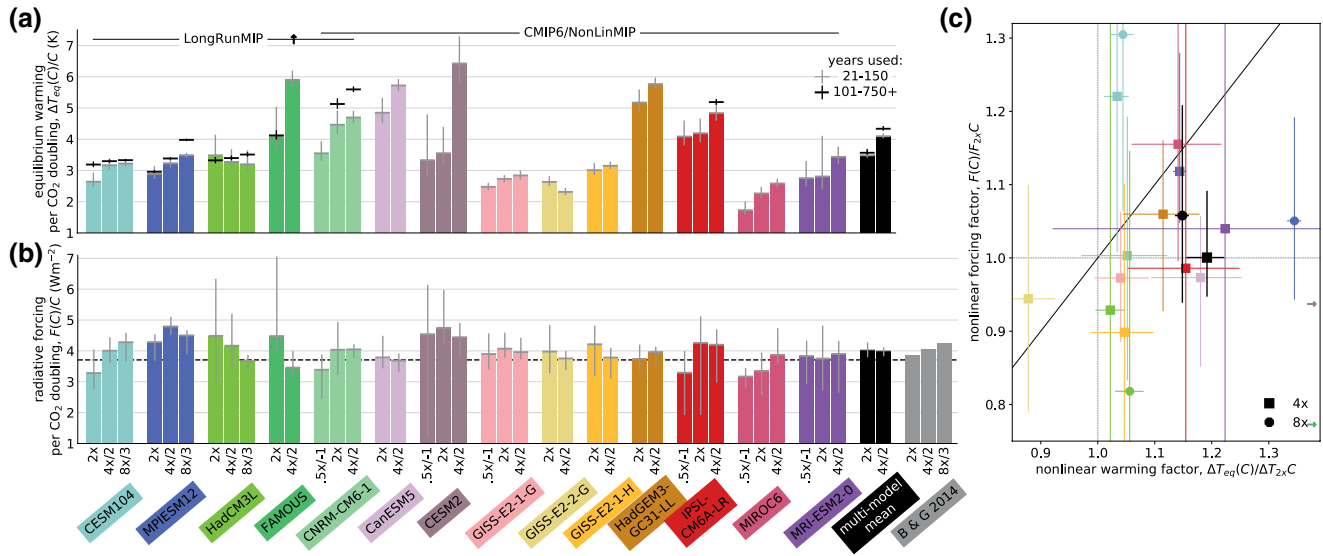


Figure 1. (a) Equilibrium warming per CO₂ doubling ($\Delta T_{eq}(C)/C$) for abrupt $-2^C \times$ simulations estimated using years 21–150 (colored bars and gray horizontal lines) and years 101– n (where n is at least 750 years and given in Table S2; black horizontal lines). Vertical lines in panels a and b and all lines in panel c give the 2.5th–97.5th percentile range of uncertainty (see Text S1). FAMOUS abrupt $4 \times$ CO₂ is an outlier, with $\Delta T_{4x}/2 = 7.6K$ when 1,000 years are used. (b) Radiative forcing per CO₂ doubling ($F(C)/C$) for abrupt $-2^C \times$ simulations estimated using years 1–10 (colored bars and gray horizontal lines). The dashed black line shows the Myhre et al. (1998) assumption of linear $F(C)$, while the gray bars give the analytic formula from Byrne and Goldblatt (2014). (c) Colored squares (octagons) show the factor by which equilibrium warming and forcing for an abrupt $4 \times$ CO₂ (abrupt $8 \times$ CO₂) simulation exceeds the linear extrapolation of its model's abrupt $2 \times$ CO₂ values. Colors are the same as panels (a) and (b). FAMOUS and CESM2 4X have nonlinear warming factors greater than 1.8.

Under preindustrial concentrations, the spectral line shape of CO₂ absorption bands creates a logarithmic dependence of N on changes in pCO_2 , so that the *forcing per CO₂ doubling* ($\tilde{F} \equiv \partial N / \partial C$) is often assumed to be constant (Myhre et al., 1998). Our definition of radiative forcing also includes adjustments of the atmosphere, land, and ocean to CO₂ changes that occur independently of subsequent changes in surface temperature (e.g., Kamae et al., 2015; Sherwood et al., 2014). This “effective radiative forcing” is also often assumed to be constant per CO₂ doubling (Forster et al., 2016), as is the radiative feedback (Gregory et al., 2004; Hansen et al., 1985). Substituting these constant terms into Equation 5, we can solve for $\Delta T_{eq}(C)$:

$$\Delta T_{eq}(C) = -\frac{\tilde{F}}{\lambda} C \quad (6)$$

Assuming a constant \tilde{F} and λ is equivalent to approximating $N(T, C)$ with the linear Taylor expansion of N around preindustrial values of C_{pi} and T_{pi} (i.e., $N(C, T) \approx \tilde{F}C + \lambda\Delta T$, where $C = \Delta C$ because $C_{pi} = 0$). The linear approximation of Equation 6 is ubiquitous in climate science (e.g., Knutti et al., 2017; Stocker et al., 2013).

The linear approximation implies that the *equilibrium climate sensitivity* (ΔT_{2x}), the equilibrium warming per CO₂ doubling, is simply $-\tilde{F} / \lambda$, which, being a ratio of two constants, is itself a constant. It should therefore not matter how many CO₂ doublings are used to estimate it since $\Delta T_{2x} = \Delta T_{eq}(C_1)/C_1 = \Delta T_{eq}(C_2)/C_2$. Figure 1a shows instead that our estimates of $\Delta T_{eq}(C)/C$ increase with CO₂ concentration for 13 of 14 models. Colored bars show estimates made by extrapolating regressions of years 21–150 of N against ΔT to equilibrium ($N = 0$) for abrupt $2^C \times$ CO₂ simulations (Gregory et al., 2004, see also solid gray lines in Figure S1). In these estimates, N and ΔT are anomalies: for LongRunMIP, we subtract the model's control simulation's mean value; for CMIP6, we subtract the linear fit of the control simulation after the branch point for the abrupt $n \times$ CO₂ simulations. We use only one ensemble member for each simulation.

Estimates of ΔT_{eq} typically increase with simulation length (Dai et al., 2020; Dunne et al., 2020; Rugenstein et al., 2020). While most CMIP6 simulations are only 150 years long, some are longer, and the LongRun-MIP models are all at least 1,000 years long. Black horizontal lines in Figure 1a show estimates using years 101–750+ (see Table S2 for exact number of years). Here and in the following we use bootstrapping to

estimate the 2.5th to 97.5th percentile range of uncertainty (gray and black vertical lines in Figure 1; see Text S1). Black bars show multimodel mean values for the two experiments for which we have simulations of all models.

The sensitivity definition in Figure 1a (i.e., $\Delta T_{2x}(C) \equiv \Delta T_{eq}(C)/C$) is often used to estimate ΔT_{2x} from abrupt $4 \times \text{CO}_2$ simulations, which our results suggest would lead to an average overestimate of at least 0.5K, even neglecting the outlier of FAMOUS. Equivalently, the nonlinearity of N leads to an average increase in equilibrium warming of at least 1K under $4 \times \text{CO}_2$. Sherwood et al. (2020) suggested that using only the first 150 years to estimate ΔT_{eq} of an abrupt $4 \times \text{CO}_2$ simulation compensates for this overestimate. For our five models with 1,000+ year abrupt $2 \times \text{CO}_2$ simulations, this compensation does not hold individually (CNRM-CM6-1's ΔT_{2x} would be 0.4K too small, FAMOUS's 1.8K too large), or on average (an 8% overestimate). If we define sensitivity instead as the equilibrium warming caused by successive CO_2 doublings ($\Delta T_{2x}(C) \equiv \Delta T_{eq}(C) - \Delta T_{eq}(C-1)$; Jonko et al., 2013), then changes in sensitivity are larger, with increases larger than 1K for seven models (Figure S2). Alternatively, if we define sensitivity as the warming from doubling CO_2 relative to preindustrial conditions only ($\Delta T_{2x} \equiv \Delta T_{eq}(1)$; e.g., Ceppi & Gregory, 2017; Knutti et al., 2017), our results suggest that this metric may have a limited applicability.

The above shows that the equilibrium climate sensitivity is inconstant, and thus the linear approximation is inaccurate. To understand the increase in sensitivity, we take the quadratic Taylor expansion of N around (C_{pi}, T_{pi}) :

$$N(C, T) \approx \frac{\partial N}{\partial C} \Big|_{C=C_{pi}, T=T_{pi}} C + \frac{\partial N}{\partial T} \Big|_{C=C_{pi}, T=T_{pi}} \Delta T + \frac{1}{2} \left(\frac{\partial^2 N}{\partial C^2} C^2 + \frac{\partial^2 N}{\partial T^2} (\Delta T)^2 + 2 \frac{\partial^2 N}{\partial C \partial T} C \Delta T \right) \quad (7)$$

Substituting these new terms into Equation 5, we have:

$$\left(\tilde{F}_{pi} + \frac{1}{2} \partial_C \tilde{F} C \right) C = - \left(\lambda_{pi} + \partial_C \lambda C + \frac{1}{2} \partial_T \lambda \Delta T_{eq} \right) \Delta T_{eq} \quad (8)$$

where $\tilde{F}_{pi} \equiv \frac{\partial N}{\partial C} \Big|_{C_{pi}, T_{pi}}$ and $\lambda_{pi} \equiv \frac{\partial N}{\partial T} \Big|_{C_{pi}, T_{pi}}$ are the *preindustrial forcing per CO_2 doubling* and *preindustrial feedback*, respectively, $\partial_C \tilde{F} \equiv \frac{\partial^2 N}{\partial C^2}$ is the CO_2 dependence of the forcing per doubling (which we call the *nonlinear forcing*), $\partial_C \lambda \equiv \frac{\partial^2 N}{\partial C \partial T}$ is the *feedback CO_2 dependence*, and $\partial_T \lambda \equiv \frac{\partial^2 N}{\partial T^2}$ is the *feedback temperature dependence*.

The three nonlinear terms ($\partial_C \tilde{F}$, $\partial_C \lambda$, and $\partial_T \lambda$) can all cause the equilibrium climate sensitivity to change with CO_2 concentration. Solving for $\Delta T_{eq}(C)$, we have

$$\Delta T_{eq}(C) = \frac{-\left(\lambda_{pi} + \partial_C \lambda C\right) - \sqrt{\left(\partial_C \lambda^2 - \partial_T \lambda \partial_C \tilde{F}\right) C^2 + 2\left(\lambda_{pi} \partial_C \lambda - \tilde{F}_{pi} \partial_T \lambda\right) C + \lambda_{pi}^2}}{\partial_T \lambda} \quad (9)$$

We ignore the other quadratic solution, which gives an unstable equilibrium for C . In the following sections, we consider the impact of these terms on ΔT_{eq} .

3. Radiative Forcing

Direct forcing depends linearly on C for small C (Myhre et al., 1998, who estimate $F(C) = 3.71 C \text{ Wm}^{-2}$; dashed black line, Figure 1b). At higher CO_2 levels, new absorption bands make this dependence superlinear (Byrne & Goldblatt, 2014; Etminan et al., 2016). Using the left side of Equation 8, we have

$$F(C_{pi}, T_{pi}, C) = \tilde{F}_{pi} C + \frac{1}{2} \partial_C \tilde{F} C^2 \quad (10)$$

Byrne and Goldblatt (2014) used line-by-line radiative calculations and a simple stratospheric adjustment model to estimate $F_{pi} = 3.69 \text{ Wm}^{-2}$ and $\partial_C \tilde{F} = 0.375 \text{ Wm}^{-2}$ for $0.7 \times \text{CO}_2$ – $36 \times \text{CO}_2$, implying an increase in forcing per doubling with CO_2 concentration (gray bars in Figure 1b).

We estimate forcing per doubling for each simulation (colored bars, Figure 1b) by regressing the first 10 years of N versus ΔT to $\Delta T = 0$ (dashed black lines in Figure S1; Gregory et al., 2004). This estimate includes adjustments as well as direct effects. Forcing per doubling decreases with C about as often as it increases, so that nonlinear forcing cannot explain the general increase in sensitivity. For CO_2 levels for which we have simulations for all models ($2 \times \text{CO}_2$ and $4 \times \text{CO}_2$), the multimodel mean forcing per doubling slightly decreases with C , although this decrease is not statistically significant.

Sensitivity increases with CO_2 concentration by a greater factor than forcing per doubling for most models (Figure 1c). While all simulations but one have superlinear warming (i.e., are right of the vertical dashed line), nine simulations have sublinear forcing (i.e., are below the horizontal dashed line). Thirteen out of seventeen simulations have a smaller forcing increase than a warming increase (i.e., fall below the 1-to-1 line), as do the multimodel means. Moreover, there is little correlation between the nonlinear warming and forcing factors ($R^2 = 0.05$), even ignoring models with anomalous sensitivity increases (FAMOUS and CESM2; $R^2 = 0.14$). Forcing does not play a large role in the sensitivity increase for most models, although it may for individual models (e.g., CESM1.0.4).

Using 20 years instead of 10 to estimate F reduces uncertainty (Figure S3a) but biases estimates of F low because of an increase in the slope of N versus ΔT over time (Figure S3b) and has little effect on our findings in Figure 1c (see Figure S3c). Sensitivity also increases by a greater factor than would be implied by Byrne and Goldblatt (2014) (Figure S3d). Our findings are also the same if we first estimate \tilde{F}_{pi} and $\partial_C \tilde{F}$ for each model by fitting the quadratic function in Equation 10 (Figures S4a and S4b): $\partial_C \tilde{F}$ is positive for only half of the models, with multimodel mean values of $\tilde{F}_{pi} = 4.01 \text{ Wm}^{-2}$ and $\partial_C \tilde{F} = 0.017 \text{ Wm}^{-2}$.

4. Radiative Feedback

If sensitivity is not proportional to forcing, then Equation 5 implies the feedback is inconstant. Inconstant feedbacks are commonly associated with the “pattern effect,” in which the slope of N versus ΔT under constant forcing varies. This slope is a weighted average of the spatial pattern of feedbacks, where the weights are given by the spatial pattern of surface warming. The warming pattern evolves primarily due to the delay of warming in regions of deep ocean heat uptake (e.g., Andrews et al., 2015; Armour et al., 2013; Bloch-Johnson et al., 2020; Dong et al., 2019; Rose et al., 2014; Rugenstein et al., 2016; Senior & Mitchell, 2000; Zhou et al., 2017).

The framework in Section 2 does not account for spatially varying feedbacks, which make $N(C, T)$ an ill-defined function, in that it can have multiple values: the same globally averaged T with warmer temperatures in regions with strong negative feedbacks implies a lower N than if the surface temperature was spatially uniform. It is more accurate to define $N(C, \vec{T})$, where \vec{T} is the spatial temperature pattern (Haugstad et al., 2017). This means that the equilibrium response cannot generally be estimated from the slope of N versus ΔT , which may evolve differently at different forcing levels simply because the patterns of warming associated with each simulation are different. For example, it is possible for the slope of N versus ΔT to change due to a pattern effect, but for the overall response to forcing to be linear, so that the equilibrium climate sensitivity is constant (Rohrschneider et al., 2019).

To create a tractable framework, we assume that every globally averaged surface temperature T is associated with a unique equilibrium pattern, $\vec{T}_{eq}(T)$, which is the pattern when T is in equilibrium (stable or unstable) for some C . We then substitute N with $N_{eq}(C, T) \equiv N(C, \vec{T}_{eq}(T))$ in our above definitions of λ and F . This substitution does not affect our forcing definition, as forcing is typically defined with respect to an equilibrated state but ensures that any change in the feedback implies a change in the proportionality of $F(C)$ to $\Delta T_{eq}(C)$, and vice versa, as expected from Equation 5. It also causes λ to vary far less with T than suggested by the slope of N versus T (Figure S1) since changes in the equilibrium pattern of warming are much smaller than the time-evolution of the transient warming pattern.

From Equation 8, we have:

$$\lambda(C, T) = \lambda_{pi} + \partial_C \lambda C + \partial_T \lambda \Delta T \quad (11)$$

where $\lambda_{pi} \equiv \partial N / \partial T|_{pi}$ is the preindustrial feedback, $\partial_C \lambda \equiv \partial \lambda / \partial C = \partial^2 N / \partial C \partial T$ represents the feedback CO₂ dependence, and $\partial_T \lambda \equiv \partial \lambda / \partial T = \partial^2 N / \partial T^2$ represents the feedback temperature dependence (Bloch-Johnson et al., 2015; Roe & Armour, 2011).

Feedback CO₂ dependence quantifies the effect of additional atmospheric CO₂ on radiative feedbacks, such as damping the Planck feedback by making more frequencies optically thick (Seeley & Jeevanjee, 2020). It can also include effects due to forcing adjustments. The pattern effect prevents us from comparing the slope of N versus ΔT across forcing levels to estimate $\partial_C \lambda$. Instead, we use additional experiments for five coupled AOGCMs, CESM1.2.2, CESM2*, CNRM-CM6-1*, HadGEM2, and HadGEM3-GC31-LL* (starred models are from our main analysis; see Table S3 and Text S2), to estimate $\partial_C \lambda$. Since $\partial \lambda / \partial C \equiv \partial^2 N / \partial C \partial T = \partial \tilde{F} / \partial T$, feedback CO₂ dependence is also the dependence of the forcing per doubling on the reference temperature. We use pairs of experiments initialized at a colder temperature (T_{cold}) and a warmer temperature (T_{warm}) and the same initial CO₂ concentration C_i to estimate forcing from the same amount of CO₂ doubling C :

$$\partial_C \lambda = \partial_T \tilde{F} \approx \frac{1}{\Delta T} \frac{\Delta F(C_i, T_i, C)}{C} = \frac{F_{warm} - F_{cold}}{(T_{warm} - T_{cold})C} \quad (12)$$

where $F_{warm} \equiv F(C_i, T_{warm}, C)$ and $F_{cold} \equiv F(C_i, T_{cold}, C)$.

F_{cold} and F_{warm} can be estimated using pairs of abrupt simulations (i.e., an abrupt $4 \times \text{CO}_2$ simulation to estimate F_{cold} , and a simulation where CO₂ is abruptly lowered from $4 \times \text{CO}_2$ to preindustrial values to estimate $-F_{warm}$) or from two pairs of fixed-SST experiments (Hansen et al., 2005) at two different temperatures and CO₂ concentrations. $\partial_C \lambda$ has a multimodel mean value of $\partial_C \lambda_{mean} = 0.0256 \text{ W m}^{-2} \text{ K}^{-1}$ and a range of $0.0057\text{--}0.049 \text{ W m}^{-2} \text{ K}^{-1}$, suggesting that feedback CO₂ dependence is generally positive, increasing sensitivity with CO₂ concentration.

To estimate each model's feedback temperature dependence, we perform a least squares fit of Equation 8 using estimates of \tilde{F}_{pi} and $\partial_C \tilde{F}$ from the previous section, as well as model-specific estimates of $\partial_C \lambda$ when available or otherwise $\partial_C \lambda_{mean}$. We perform this fit using pairs of C and ΔT_{eq} for each simulation, including the pair $C = 0$ and $\Delta T_{eq} = 0$ for the control simulation, giving estimates of λ_{pi} and $\partial_T \lambda$ (colored dots, Figure 2). We find that 10 of the 14 models have positive feedback temperature dependence, with a multimodel mean value of $\partial_T \lambda_{mean} = 0.029 \text{ W m}^{-2} \text{ K}^{-2}$ and a range from -0.14 to $0.109 \text{ W m}^{-2} \text{ K}^{-2}$.

With positive feedback temperature dependence, warming increases the feedback, leading to further warming, and so on. Under sufficient forcing, runaway warming occurs (Bloch-Johnson et al., 2015; Zaliapin & Ghil, 2010), specifically when Equation 9 has no real solution ($\partial_T \lambda > (\lambda_{pi} + \partial_C \lambda C)^2 / (\partial_C \tilde{F} C^2 + 2 \tilde{F}_{pi} C)$), as shown by the light gray region for $8 \times \text{CO}_2$ and dark gray region for $4 \times \text{CO}_2$ (assuming that radiative forcing follows Byrne and Goldblatt (2014) and $\partial_C \lambda = \partial_C \lambda_{mean}$). FAMOUS falls in the latter region, and its abrupt $4 \times \text{CO}_2$ simulation does appear to lose its negative feedback (Figure S1); four models lie in the $8 \times \text{CO}_2$ runaway region. Climates in the gray regions do not actually warm infinitely, but simply warm sufficiently that the quadratic approximation breaks. Higher-order terms determine the temperature at which stability is regained, or if stability is lost in the first place. Models close to these runaway regions experience a sensitivity increase at the associated forcing level: the six models with black outlines experience an estimated increase of equilibrium warming under $8 \times \text{CO}_2$ of at least 3K, given each model's forcing and $\partial_C \lambda$ estimates.

High estimated sensitivity ($\Delta T_{4x}/2 > 4.5\text{K}$) has been found in 20 CMIP6 models (Table S4). Of the six models with $\Delta T_{4x}/2 > 4.5\text{K}$ that appear in our study (i.e., models right of the dotted line in Figure 2), four have $\Delta T_{2x} < 4.5\text{K}$ (i.e., are left of the dashed line). These models reconcile the moderate ΔT_{2x} implied by observations, paleoclimate, and processed-based analysis (Sherwood et al., 2020) with the sensitivity increases seen in paleoclimate studies of the warm Cenozoic (Anagnostou et al., 2016; Caballero & Huber, 2013; Farnsworth et al., 2019; Pierrehumbert, 2013; Shaffer et al., 2016).

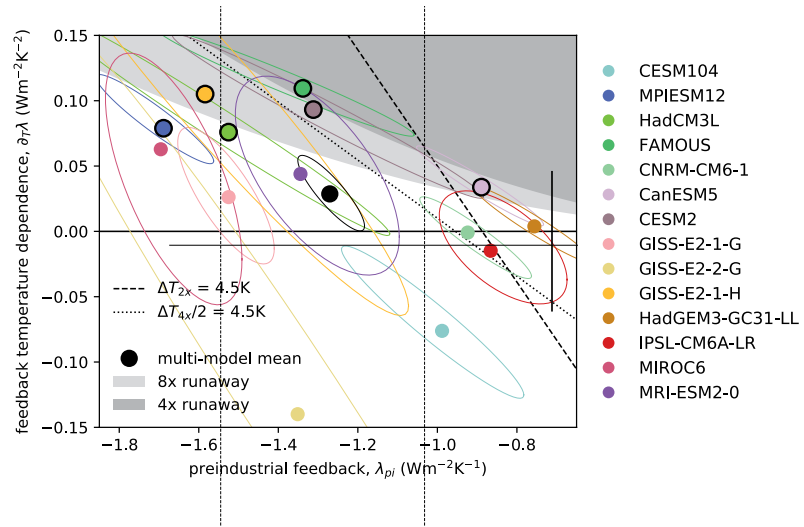


Figure 2. Preindustrial feedback versus feedback temperature dependence (colored dots; colored ellipsoids give the 75th percentile of uncertainty). Values in the dark (light) gray region imply runaway warming under $4 \times \text{CO}_2$ ($8 \times \text{CO}_2$) and values above the dashed (dotted) black line have a sensitivity estimated from abrupt $2 \times \text{CO}_2$ (abrupt $4 \times \text{CO}_2$) above 4.5K. All thresholds are calculated assuming forcing from Byrne and Goldblatt (2014) and model-mean feedback CO_2 dependence. Colored dots with black outlines experience an additional 3K of equilibrium warming under $8 \times \text{CO}_2$ given our estimate of that model's forcing and $\partial_C \lambda$.

To test the assumptions behind Figure 2, we recalculate it with default values of $\partial_C \lambda = 0$ and $0.05 \text{ W m}^{-2} \text{ K}^{-1}$ (Figures S5a and S5b, respectively). This shifts the estimates of $\partial_T \lambda$ in the opposite direction as $\partial_C \lambda$, but also shifts the thresholds in the same manner, so that qualitatively the results are unchanged. Estimating forcing using years 1–20 instead of 1–10 has little effect (Figure S5c), so does using the direct estimate of $F(C)$ instead of $\left(\tilde{F}_{pi} + \frac{1}{2} \partial_C \tilde{F} C \right) C$ on the left side of Equation 8 (Figure S5d). Figure S5e shows how $\partial_T \lambda$ evolves as more years are used to estimate the equilibrium warming. While more years do not greatly affect the results relative to each other, using years 101–1,000 instead of 21–150 increases the magnitude of $\partial_T \lambda$ (excepting FAMOUS, which appears to be in a state of runaway). Since feedback temperature dependence should continue to affect the slope of N versus ΔT beyond year 150 (Rugenstein et al., 2020), our estimates of CMIP6 models' $|\partial_T \lambda|$ and sensitivity changes may both be biased low.

5. Causes of Sensitivity Increases

Figure 3a compares the contribution of the three nonlinear terms to each model's change in equilibrium climate sensitivity, $\Delta \Delta T_{2x} \equiv \Delta T_{4x}/2 - \Delta T_{2x}$. Using Equation 9 to express equilibrium warming as a function of the quadratic approximation coefficients, $\Delta T_{eq}(C; \tilde{F}_{pi}, \lambda_{pi}, \partial_C \tilde{F}, \partial_C \lambda, \partial_T \lambda)$, we define:

$$\Delta \Delta T_{2x, \partial_C \tilde{F}} \equiv \Delta T_{eq}(2; \tilde{F}_{pi}, \lambda_{pi}, \partial_C \tilde{F}, 0, 0) / 2 - \Delta T_{eq}(1; \tilde{F}_{pi}, \lambda_{pi}, \partial_C \tilde{F}, 0, 0) \quad (13)$$

$$\Delta \Delta T_{2x, \partial_C \lambda} \equiv \Delta T_{eq}(2; \tilde{F}_{pi}, \lambda_{pi}, 0, \partial_C \lambda, 0) / 2 - \Delta T_{eq}(1; \tilde{F}_{pi}, \lambda_{pi}, 0, \partial_C \lambda, 0) \quad (14)$$

$$\Delta \Delta T_{2x, \partial_T \lambda} \equiv \Delta T_{eq}(2; \tilde{F}_{pi}, \lambda_{pi}, 0, 0, \partial_T \lambda) / 2 - \Delta T_{eq}(1; \tilde{F}_{pi}, \lambda_{pi}, 0, 0, \partial_T \lambda) \quad (15)$$

Feedback temperature dependence is the dominant term for the three models with the largest sensitivity increases, accounts for 69% of the average increase and contributes the largest term to the median increase (where FAMOUS is excluded from the averages, as the quadratic model suggests it experiences runaway warming under $4 \times \text{CO}_2$). Feedback CO_2 dependence contributes a small, positive increase in sensitivity, while nonlinear forcing decreases sensitivity about as much and as often as it increases it.

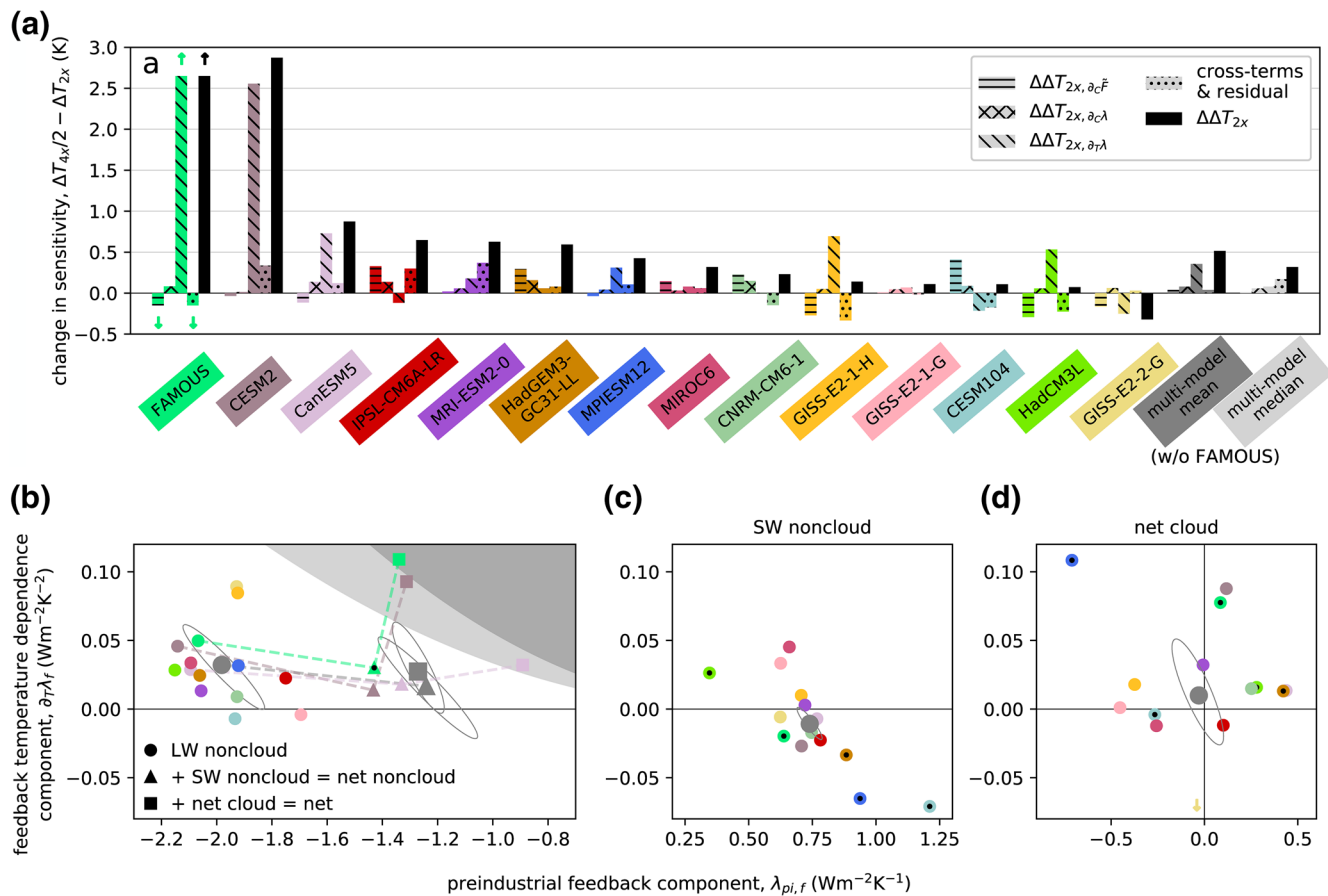


Figure 3. (a) Contributions to the change in sensitivity from $2 \times \text{CO}_2$ to $4 \times \text{CO}_2$ (black bars) from nonlinear forcing ($\partial_c \tilde{F}$, horizontally hatched bars), feedback CO₂ dependence ($\partial_c \lambda$, crossed-hatched bars), and feedback temperature dependence ($\partial_T \lambda$, diagonally hatched bars). Dotted bars represent cross-terms, higher-order nonlinearities, and errors in our estimates. FAMOUS is not included in the mean and median as the quadratic model suggests it is in a state of runaway under $4 \times \text{CO}_2$. (b), (c), and (d) Colored circles give estimates of the longwave (LW) noncloud, shortwave (SW) noncloud, and net cloud components, respectively, of the preindustrial feedback and feedback temperature dependence. Models with dotted circles use clear-sky fluxes instead of approximate partial radiative perturbation to partition the SW flux into noncloud and cloud components. Colors are given by the model names in panel a. Gray circles give the multimodel mean and gray ellipsoids give the estimated 75th percentile of uncertainty. The shaded regions in panel b are as in Figure 2. Triangles in panel b show the result of adding the SW noncloud component to LW noncloud components. Squares show the result for additionally adding the net cloud component.

To better understand these sensitivity increases, we estimate the flux components of the preindustrial feedback and feedback temperature dependence (Figures 3b–3d; see Figure S6 for all components and uncertainties) by substituting individual top-of-atmosphere fluxes for N in the above derivations (see Text S3). We consider longwave (LW) versus shortwave (SW) and noncloud versus cloud components. For LW fluxes, noncloud versus cloud components are estimated using clear-sky fluxes and cloud radiative effect. For SW fluxes, to avoid cloud masking (Soden et al., 2004) we instead use approximate partial radiative perturbation (APRP; Taylor et al., 2007) for models with sufficient data available, including most CMIP6 models. For all other models, we use clear-sky fluxes and cloud radiative effect as with the LW.

The LW noncloud feedback typically has positive temperature dependence (colored circles, Figure 3b) due to an increasing water vapor feedback (Colman & McAvaney, 2009; Crucifix, 2006; Meraner et al., 2013). While some studies found that this increase is balanced by a strengthening negative lapse rate feedback (Boer et al., 2005; Caballero & Huber, 2013; Colman & McAvaney, 2009; Yoshimori et al., 2009), in recent studies, the water vapor feedback dominates (Block & Mauritsen, 2013; Jonko et al., 2013; Meraner et al., 2013; Rieger et al., 2017), and Meraner et al. (2013) found a positive $\partial_T \lambda_{\text{LWnoncloud}}$ for most CMIP5 models. Our findings contradict recent papers that find a constant LW clear-sky feedback (Koll & Cronin, 2018; Zhang et al., 2020), though we agree that the value of the preindustrial feedback is likely close to $-2 \text{ W m}^{-2} \text{ K}^{-1}$.

The SW noncloud feedback (colored circles, Figure 3c) is the sum of a surface term (Figure S6e) and an atmosphere term (Figure S6f). The former represents a positive ice albedo feedback, which typically saturates, giving a negative temperature dependence (Block & Mauritsen, 2013; Colman & McAvaney, 2009; Duan et al., 2019; Jonko et al., 2013; Meraner et al., 2013; Rieger et al., 2017). The noncloud atmosphere term represents a positive water vapor feedback, which typically has a positive temperature dependence. Their sum has a positive preindustrial feedback with negligible temperature dependence (Figure 3c). The SW noncloud outliers are models for which clear-sky fluxes were used instead of APRP (circles with black dots, Figure 3c). Comparison of clear-sky versus APRP estimates of the SW noncloud component suggests that cloud masking biases generally increases the uncertainty of the SW noncloud component (Figures S6c vs. S6g).

While the cloud feedback has multimodel mean values close to zero, it has more intermodel spread than the other two components (Figure 3d) and has positive temperature dependence for most models. For CESM2, this occurs because its negative mixed-phase cloud feedback saturates (Bjordal et al., 2020; Frey & Kay, 2018; Tan et al., 2016). The spread in cloud feedback explains the range of nonlinearity in Figure 3a. The average LW noncloud feedback on its own (gray circle in Figure 3b) would experience too little warming for its temperature dependence to matter (e.g., $\Delta\Delta T_{2x} = \Delta T_{4x}/2 - \Delta T_{2x} \approx 0.17\text{K}$ assuming forcing from Byrne and Goldblatt (2014) and average $\partial_c\lambda$). Adding the SW noncloud feedback does not change the temperature dependence but makes the preindustrial feedback more positive (gray triangle in Figure 3b), causing more warming, increasing the nonlinearity (e.g., $\Delta\Delta T_{2x} \approx 0.33\text{K}$ using the same assumptions). Adding the average cloud feedback causes little change (gray square in Figure 3b). For individual models, cloud feedbacks can move the climate into nonlinear regions, either by increasing the preindustrial feedback (CanESM5) or by increasing the feedback temperature dependence (CESM2 and FAMOUS). On the other hand, GISS-E2-2-G's cloud feedback temperature dependence is anomalously negative, and, therefore, it is the only model for which sensitivity decreases with CO₂ concentration.

We briefly discuss the flux components of the other two nonlinear terms (Figure S7). The LW clear-sky term of the nonlinear forcing is negative for 11 of 14 models (Figure S7a). Since the direct LW clear-sky forcing depends superlinearly on CO₂ doubling (Byrne & Goldblatt, 2014), this negative term is due either to oversimplifications in the model's radiative scheme or to adjustments. The other components vary in sign, with the largest source of intermodel spread coming from the cloud components. Since APRP accounts for cloud masking, the SW cloud spread must also be due to forcing adjustments. Adjustments thus play a first-order role in determining nonlinear forcing. The LW clear-sky component of feedback CO₂ dependence is positive for all five models (Figure S7b), likely due to a blocked Planck feedback. SW cloud contributes the largest source of intermodel spread, so that forcing adjustments also play a first-order role in this nonlinearity.

6. Conclusions

Equilibrium climate sensitivity increases with CO₂ concentration for 13 of 14 models, contradicting the linear approximation of global energy balance, which assumes a constant forcing per CO₂ doubling and a constant radiative feedback. On average, climate models experience at least a degree of additional equilibrium warming under $4 \times \text{CO}_2$ due to this sensitivity increase. Using a quadratic approximation allows us to capture the sensitivity increase using three second-order terms: nonlinear forcing, feedback CO₂ dependence, and feedback temperature dependence.

Feedback temperature dependence explains 69% of the sensitivity increase and explains more of the median increase than any other term. Most importantly, it explains the particularly large increase seen in a handful of models, as positive feedback temperature dependence can cause runaway increases in sensitivity. Four models are predicted to experience runaway warming under CO₂ concentrations eight times larger than the preindustrial, and six models are projected to experience at least three additional degrees of equilibrium warming under this concentration. Feedback temperature dependence plays a key role in determining the risk of extreme warming in the coming centuries.

Out of 14, 10 models have positive feedback temperature dependence, primarily due to the LW clear-sky feedback. Models with large sensitivity increases have cloud feedbacks with either anomalously positive temperature dependence or anomalously positive preindustrial values. Feedback CO₂ dependence plays a

smaller role, but results from five models suggest that it is likely positive, increasing sensitivity, primarily due to its LW clear-sky component. The forcing per CO₂ doubling decreases with CO₂ concentration for as many models as it increases. Nonlinear forcing contributes less to the sensitivity increase than either other term, although it can be important for individual models. Forcing adjustments play a first-order role in determining the nonlinear forcing.

The substantial uncertainties in some of the terms discussed here could be greatly decreased with additional simulations. Longer simulations give better estimates of equilibrium warming (Dai et al., 2020; Dunne et al., 2020; Rugenstein et al., 2020); fixed-SST experiments give better radiative forcing estimates (Forster et al., 2016; Pincus et al., 2016); and simulations at multiple CO₂ levels allow for an assessment of nonlinearities (Good et al., 2016). Simulations that behave in surprising or anomalous ways may be exhibiting nonlinear dynamics, and should not be neglected (Valdes, 2011). Even if a loss of stability causes models to warm outside the range for which they were calibrated, the increase in sensitivity may still be physical. Exploring and documenting the nonlinear frontiers of warming in climate models is essential to assessing the risk of extreme warming for the real world.

Data Availability Statement

CMIP6 data are at <https://pcmdi.llnl.gov/CMIP6/>. LongRunMIP data access is at <http://www.longrunmip.org/>.

Acknowledgments

The authors thank Tim Andrews for making the HadGEM3-GC3.1-LL abrupt $-2 \times \text{CO}_2$ simulation available at <https://github.com/timothyandrews/abrupt-2xCO2>. This project has received funding from the European Research Council (ERC) under the European Union's Horizon 2020 research and innovation program (grant agreement No. 786427, project "Couplet" and grant agreement No. 820829, project "CONSTRAIN").

References

- Anagnostou, E., John, E. H., Babila, T. L., Sexton, P. F., Ridgwell, A., Lunt, D. J., et al. (2020). Proxy evidence for state-dependence of climate sensitivity in the Eocene greenhouse. *Nature Communications*, *11*(1), 4436. <https://doi.org/10.1038/s41467-020-17887-x> (Number: 1 Publisher: Nature Publishing Group).
- Anagnostou, E., John, E. H., Edgar, K. M., Foster, G. L., Ridgwell, A., Inglis, G. N., et al. (2016). Changing atmospheric CO₂ concentration was the primary driver of early Cenozoic climate. *Nature*, *533*(7603), 380–384. <https://doi.org/10.1038/nature17423>
- Andrews, T., Gregory, J. M., & Webb, M. J. (2015). The dependence of radiative forcing and feedback on evolving patterns of surface temperature change in climate models. *Journal of Climate*, *28*(4), 1630–1648. <https://doi.org/10.1175/JCLI-D-14-00545.1>
- Armour, K. C., Bitz, C. M., & Roe, G. H. (2013). Time-varying climate sensitivity from regional feedbacks. *Journal of Climate*, *26*(13), 4518–4534. <https://doi.org/10.1175/JCLI-D-12-00544.1>
- Bitz, C. M., Shell, K. M., Gent, P. R., Bailey, D. A., Danabasoglu, G., Armour, K. C., et al. (2012). Climate sensitivity of the community climate system model, version 4. *Journal of Climate*, *25*(9), 3053–3070. <https://doi.org/10.1175/JCLI-D-11-00290.1>
- Bjorndal, J., Storelvmo, T., Alterskjær, K., & Carlsen, T. (2020). Equilibrium climate sensitivity above 5°C plausible due to state-dependent cloud feedback. *Nature Geoscience*, *13*(11), 718–721. <https://doi.org/10.1038/s41561-020-00649-1> (Number: 11 Publisher: Nature Publishing Group).
- Bloch-Johnson, J., Pierrehumbert, R. T., & Abbot, D. S. (2015). Feedback temperature dependence determines the risk of high warming. *Geophysical Research Letters*, *42*(12), 4973–4980. <https://doi.org/10.1002/2015GL064240>
- Bloch-Johnson, J., Rugenstein, M., & Abbot, D. S. (2020). Spatial radiative feedbacks from internal variability using multiple regression. *Journal of Climate*, *33*(10), 4121–4140. <https://doi.org/10.1175/JCLI-D-19-0396.1> (Publisher: American Meteorological Society).
- Block, K., & Mauritsen, T. (2013). Forcing and feedback in the MPI-ESM-LR coupled model under abruptly quadrupled CO₂. *Journal of Advances in Modeling Earth Systems*, *5*(4), 676–691. <https://doi.org/10.1002/jame.20041>
- Boer, G. J., Hamilton, K., & Zhu, W. (2005). Climate sensitivity and climate change under strong forcing. *Climate Dynamics*, *24*(7), 685–700. <https://doi.org/10.1007/s00382-004-0500-3>
- Byrne, B., & Goldblatt, C. (2014). Radiative forcing at high concentrations of well-mixed greenhouse gases. *Geophysical Research Letters*, *41*(1), 152–160. <https://doi.org/10.1002/2013GL058456>
- Caballero, R., & Huber, M. (2013). State-dependent climate sensitivity in past warm climates and its implications for future climate projections. *Proceedings of the National Academy of Sciences*, *110*(35), 14162–14167. <https://doi.org/10.1073/pnas.1303365110>. Retrieved from <http://www.pnas.org/content/110/35/14162>
- Ceppi, P., & Gregory, J. M. (2017). Relationship of tropospheric stability to climate sensitivity and Earth's observed radiation budget. *Proceedings of the National Academy of Sciences*, *114*(50), 13126–13131. <https://doi.org/10.1073/pnas.1714308114>. Retrieved from <http://www.pnas.org/content/114/50/13126>
- Colman, R., & McAvaney, B. (2009). Climate feedbacks under a very broad range of forcing. *Geophysical Research Letters*, *36*(1). <https://doi.org/10.1029/2008GL036268>
- Crucifix, M. (2006). Does the last glacial maximum constrain climate sensitivity? *Geophysical Research Letters*, *33*, L18701. <https://doi.org/10.1029/2006GL027137>
- Dai, A., Huang, D., Rose, B. E. J., Zhu, J., & Tian, X. (2020 April). Improved methods for estimating equilibrium climate sensitivity from transient warming simulations. *Climate Dynamics*, *54*(11–12), 4515–4543. <https://doi.org/10.1007/s00382-020-05242-1>
- Dong, Y., Proistosescu, C., Armour, K. C., Battisti, D. S., Dong, Y., Proistosescu, C., et al. (2019). Attributing historical and future evolution of radiative feedbacks to regional warming patterns using a green's function approach: The preeminence of the Western Pacific. *Journal of Climate*, *32*(17), 5471–5491. <https://doi.org/10.1175/JCLI-D-18-0843.1>
- Duan, L., Cao, L., & Caldeira, K. (2019). Estimating contributions of sea ice and land snow to climate feedback. *Journal of Geophysical Research: Atmospheres*, *124*(1), 199–208. <https://doi.org/10.1029/2018JD029093>

- Dunne, J. P., Winton, M., Bacmeister, J., Danabasoglu, G., Gettelman, A., Golaz, J.-C., et al. (2020). Comparison of equilibrium climate sensitivity estimates from slab ocean, 150-year, and longer simulations. *Geophysical Research Letters*, *47*(16), e2020GL088852. <https://doi.org/10.1029/2020GL088852>
- Etminan, M., Myhre, G., Highwood, E. J., & Shine, K. P. (2016). Radiative forcing of carbon dioxide, methane, and nitrous oxide: A significant revision of the methane radiative forcing. *Geophysical Research Letters*, *43*(24), 12614–12623. <https://doi.org/10.1002/2016GL071930>
- Eyring, V., Bony, S., Meehl, G. A., Senior, C. A., Stevens, B., Stouffer, R. J., & Taylor, K. E. (2016). Overview of the coupled model intercomparison project phase 6 (CMIP6) experimental design and organization. *Geoscientific Model Development*, *9*(5), 1937–1958. <https://doi.org/10.5194/gmd-9-1937-2016>
- Farnsworth, A., Lunt, D. J., O'Brien, C. L., Foster, G. L., Inglis, G. N., Markwick, P., et al. (2019). Climate sensitivity on geological timescales controlled by nonlinear feedbacks and ocean circulation. *Geophysical Research Letters*, *46*(16), 9880–9889. <https://doi.org/10.1029/2019GL083574>
- Forster, P. M., Richardson, T., Maycock, A. C., Smith, C. J., Samset, B. H., Myhre, G., et al. (2016). Recommendations for diagnosing effective radiative forcing from climate models for CMIP6. *Journal of Geophysical Research: Atmospheres*, *121*(20), 12460–12475. <https://doi.org/10.1002/2016JD025320>
- Frey, W. R., & Kay, J. E. (2018). The influence of extratropical cloud phase and amount feedbacks on climate sensitivity. *Climate Dynamics*, *50*(7), 3097–3116. <https://doi.org/10.1007/s00382-017-3796-5>
- Friedrich, T., Timmermann, A., Tigchelaar, M., Timm, O. E., & Ganopolski, A. (2016). Nonlinear climate sensitivity and its implications for future greenhouse warming. *Science Advances*, *2*(11), e1501923. <https://doi.org/10.1126/sciadv.1501923>
- Good, P., Andrews, T., Chadwick, R., Dufresne, J.-L., Gregory, J. M., Lowe, J. A., et al. (2016). NonlinMIP contribution to CMIP6: Model intercomparison project for nonlinear mechanisms: Physical basis, experimental design and analysis principles (v1.0). *Geoscientific Model Development*, *9*(11), 4019–4028. <https://doi.org/10.5194/gmd-9-4019-2016>
- Gregory, J. M., Andrews, T., & Good, P. (2015). The inconstancy of the transient climate response parameter under increasing CO₂. *Philosophical Transactions of the Royal Society A: Mathematical, Physical & Engineering Sciences*, *373*(2054), 20140417. <https://doi.org/10.1098/rsta.2014.0417>
- Gregory, J. M., Ingram, W. J., Palmer, M. A., Jones, G. S., Stott, P. A., Thorpe, R. B., et al. (2004). A new method for diagnosing radiative forcing and climate sensitivity. *Geophysical Research Letters*, *31*(3), L03205. <https://doi.org/10.1029/2003GL018747>
- Hansen, J., Russell, G., Lacy, A., Fung, I., Rind, D., & Stone, P. (1985). Climate response times: Dependence on climate sensitivity and ocean mixing. *Science*, *229*(4716), 857–859. <https://doi.org/10.1126/science.229.4716.857>
- Hansen, J., Sato, M., Ruedy, R., Nazarenko, L., Lacy, A., Schmidt, G. A., et al. (2005). Efficacy of climate forcings. *Journal of Geophysical Research*, *110*, D18104. <https://doi.org/10.1029/2005JD005776>
- Haugstad, A. D., Armour, K. C., Battisti, D. S., & Rose, B. E. J. (2017). Relative roles of surface temperature and climate forcing patterns in the inconstancy of radiative feedbacks. *Geophysical Research Letters*, *44*(14), 7455–7463. <https://doi.org/10.1002/2017GL074372>
- Heydt, A. S. v. d., Dijkstra, H. A., Wal, R. S. W. v. d., Caballero, R., Crucifix, M., Foster, G. L., et al. (2016). Lessons on climate sensitivity from past climate changes. *Current Climate Change Reports*, *2*(4), 148–158. <https://doi.org/10.1007/s40641-016-0049-3>
- Hoffman, P. F., Kaufman, A. J., Halverson, G. P., & Schrag, D. P. (1998). A neoproterozoic snowball earth. *Science*, *281*(5381), 1342–1346. <https://doi.org/10.1126/science.281.5381.1342>
- Ingersoll, A. P. (1969). The runaway greenhouse: A history of water on Venus. *Journal of the Atmospheric Sciences*, *26*(6), 1191–1198. [https://doi.org/10.1175/1520-0469\(1969\)026<1191:TRGAHO>2.0.CO;2](https://doi.org/10.1175/1520-0469(1969)026<1191:TRGAHO>2.0.CO;2)
- Jonko, A. K., Shell, K. M., Sanderson, B. M., & Danabasoglu, G. (2013). Climate feedbacks in CCSM3 under changing CO₂ forcing. Part II: Variation of climate feedbacks and sensitivity with forcing. *Journal of Climate*, *26*(9), 2784–2795. <https://doi.org/10.1175/JCLI-D-12-00479.1>
- Kamae, Y., Watanabe, M., Ogura, T., Yoshimori, M., & Shiogama, H. (2015). Rapid adjustments of cloud and hydrological cycle to increasing CO₂: A review. *Current Climate Change Reports*, *1*(2), 103–113. <https://doi.org/10.1007/s40641-015-0007-5>
- Knutti, R., Rugenstein, M. A. A., & Hegerl, G. C. (2017). Beyond equilibrium climate sensitivity. *Nature Geoscience*, *10*(10), 727–736. <https://doi.org/10.1038/ngeo3017>
- Köhler, P., Stap, L. B., von der Heydt, A. S., de Boer, B., van de Wal, R. S. W., & Bloch-Johnson, J. (2017). A state-dependent quantification of climate sensitivity based on paleodata of the last 2.1 million years. *Paleoceanography*, *32*, 1102–1114. <https://doi.org/10.1002/2017PA003190>
- Koll, D. D. B., & Cronin, T. W. (2018). Earth's outgoing longwave radiation linear due to H₂O greenhouse effect. *Proceedings of the National Academy of Sciences*, *115*(41), 10293–10298. <https://doi.org/10.1073/pnas.1809868115>. Retrieved from <https://www.pnas.org/content/115/41/10293>
- Komabayasi, M. (1967). Discrete equilibrium temperatures of a hypothetical planet with the atmosphere and the hydrosphere of one component-two phase system under constant solar radiation. *Journal of the Meteorological Society of Japan. Series II*, *45*(1), 137–139. https://doi.org/10.2151/jmsj1965.45.1_137
- Kutzbach, J. E., He, F., Vavrus, S. J., & Ruddiman, W. F. (2013). The dependence of equilibrium climate sensitivity on climate state: Applications to studies of climates colder than present. *Geophysical Research Letters*, *40*(14), 3721–3726. <https://doi.org/10.1002/grl.50724>
- Martínez-Botí, M. A., Foster, G. L., Chalk, T. B., Rohling, E. J., Sexton, P. F., Lunt, D. J., et al. (2015). Plio-Pleistocene climate sensitivity evaluated using high-resolution CO₂ records. *Nature*, *518*(7537), 49–54. <https://doi.org/10.1038/nature14145>
- Meraner, K., Mauritsen, T., & Voigt, A. (2013). Robust increase in equilibrium climate sensitivity under global warming. *Geophysical Research Letters*, *40*(22), 5944–5948. <https://doi.org/10.1002/2013GL058118>
- Myhre, G., Highwood, E. J., Shine, K. P., & Stordal, F. (1998). New estimates of radiative forcing due to well mixed greenhouse gases. *Geophysical Research Letters*, *25*(14), 2715–2718. <https://doi.org/10.1029/98GL01908>
- Pierrehumbert, R. T. (2013). Hot climates, high sensitivity. *Proceedings of the National Academy of Sciences*, *110*(35), 14118–14119. <https://doi.org/10.1073/pnas.1313417110>. Retrieved from <http://www.pnas.org/content/110/35/14118>
- Pincus, R., Forster, P. M., & Stevens, B. (2016). September. The radiative forcing model intercomparison project (RFMIP): Experimental protocol for CMIP6. *Geoscientific Model Development*, *9*(9), 3447–3460. <https://doi.org/10.5194/gmd-9-3447-2016>
- Rieger, V. S., Dietmüller, S., & Ponater, M. (2017). Can feedback analysis be used to uncover the physical origin of climate sensitivity and efficacy differences? *Climate Dynamics*, *49*(7), 2831–2844. <https://doi.org/10.1007/s00382-016-3476-x>
- Roe, G. H., & Armour, K. C. (2011). How sensitive is climate sensitivity? *Geophysical Research Letters*, *38*, L14708. <https://doi.org/10.1029/2011GL047913>
- Rohrschneider, T., Stevens, B., & Mauritsen, T. (2019). On simple representations of the climate response to external radiative forcing. *Climate Dynamics*, *53*(5), 3131–3145. <https://doi.org/10.1007/s00382-019-04686-4>

- Rose, B. E. J., Armour, K. C., Battisti, D. S., Feldl, N., & Koll, D. D. B. (2014). The dependence of transient climate sensitivity and radiative feedbacks on the spatial pattern of ocean heat uptake. *Geophysical Research Letters*, *41*(3), 1071–1078. <https://doi.org/10.1002/2013GL058955>
- Rugenstein, M., Bloch-Johnson, J., Abe-Ouchi, A., Andrews, T., Beyerle, U., Cao, L., et al. (2019). LongRunMIP – Motivation and design for a large collection of millennial-length AO-GCM simulations. *Bulletin of the American Meteorological Society*, *100*(12), 2551–2570. <https://doi.org/10.1175/BAMS-D-19-0068.1>
- Rugenstein, M., Bloch-Johnson, J., Gregory, J., Andrews, T., Mauritsen, T., Li, C., et al. (2020). Equilibrium climate sensitivity estimated by equilibrating climate models. *Geophysical Research Letters*, *47*(4), e2019GL083898. <https://doi.org/10.1029/2019GL083898>
- Rugenstein, M., Gregory, J. M., Schaller, N., Sedláček, J., & Knutti, R. (2016). Multiannual ocean-atmosphere adjustments to radiative forcing. *Journal of Climate*, *29*(15), 5643–5659. <https://doi.org/10.1175/JCLI-D-16-0312.1>
- Seeley, J., & Jeevanjee, N. (2020). *H₂O windows and CO₂ radiator fins: A clear-sky explanation for the peak in ECS [preprint]*. <https://doi.org/10.1002/essoar.10503539.1>. (Archive Location: World Publisher: Earth and Space Science Open Archive Section: Atmospheric Sciences).
- Senior, C. A., & Mitchell, J. F. B. (2000). The time-dependence of climate sensitivity. *Geophysical Research Letters*, *27*(17), 2685–2688. <https://doi.org/10.1029/2000GL011373>
- Shaffer, G., Huber, M., Rondanelli, R., & Pedersen, J. O. P. (2016). Deep time evidence for climate sensitivity increase with warming. *Geophysical Research Letters*, *43*(12), 6538–6545. <https://doi.org/10.1002/2016GL069243>
- Sherwood, S. C., Bony, S., Boucher, O., Bretherton, C., Forster, P. M., Gregory, J. M., & Stevens, B. (2014). Adjustments in the forcing-feedback framework for understanding climate change. *Bulletin of the American Meteorological Society*, *96*(2), 217–228. <https://doi.org/10.1175/BAMS-D-13-00167.1>
- Sherwood, S. C., Webb, M. J., Annan, J. D., Armour, K. C., Forster, P. M., Hargreaves, J. C., et al. (2020). An assessment of Earth's climate sensitivity using multiple lines of evidence. *Reviews of Geophysics*, *58*(4), e2019RG000678. <https://doi.org/10.1029/2019RG000678>
- Snyder, C. W. (2019). Revised estimates of paleoclimate sensitivity over the past 800,000 years. *Climatic Change*, *156*(1), 121–138. <https://doi.org/10.1007/s10584-019-02536-0>
- Soden, B. J., Broccoli, A. J., & Hemler, R. S. (2004). On the use of cloud forcing to estimate cloud feedback. *Journal of Climate*, *17*(19), 3661–3665. [https://doi.org/10.1175/1520-0442\(2004\)017\(3661:OTUOCF\)2.0.CO;2](https://doi.org/10.1175/1520-0442(2004)017(3661:OTUOCF)2.0.CO;2)
- Stocker, T. F., Qin, D., Plattner, G.-K., Tignor, M., Allen, S., Boschung, J., et al. (2013). *AR5 climate change 2013: The physical science basis – IPCC (Tech. Rep.)*. Cambridge: Cambridge University Press. Retrieved from <https://www.ipcc.ch/report/ar5/wg1/>
- Stouffer, R. J., & Manabe, S. (2003). Equilibrium response of thermohaline circulation to large changes in atmospheric CO₂ concentration. *Climate Dynamics*, *20*(7), 759–773. <https://doi.org/10.1007/s00382-002-0302-4>
- Tan, I., Storelvmo, T., & Zelinka, M. D. (2016). Observational constraints on mixed-phase clouds imply higher climate sensitivity. *Science*, *352*(6282), 224–227. <https://doi.org/10.1126/science.aad5300>. Retrieved from <https://science.sciencemag.org/content/352/6282/224> (Publisher: American Association for the Advancement of Science Section: Report).
- Taylor, K. E., Crucifix, M., Braconnot, P., Hewitt, C. D., Doutriaux, C., Broccoli, A. J., et al. (2007). Estimating shortwave radiative forcing and response in climate models. *Journal of Climate*, *20*(11), 2530–2543. <https://doi.org/10.1175/JCLI4143.1> (Publisher: American Meteorological Society)
- Valdes, P. (2011). Built for stability. *Nature Geoscience*, *4*(7), 414–416. <https://doi.org/10.1038/ngeo1200>. Retrieved from <https://www.nature.com/articles/ngeo1200>
- Wolf, E. T., HaqqMisra, J., & Toon, O. B. (2018). Evaluating climate sensitivity to CO₂ across Earth's history. *Journal of Geophysical Research: Atmospheres*, *123*(21), 11861–11874. <https://doi.org/10.1029/2018JD029262>
- Yoshimori, M., Yokohata, T., & Abe-Ouchi, A. (2009). A comparison of climate feedback strength between CO₂ doubling and LGM experiments. *Journal of Climate*, *22*(12), 3374–3395. <https://doi.org/10.1175/2009JCLI2801.1>
- Zaliapin, I., & Ghil, M. (2010). Another look at climate sensitivity. *Nonlinear Processes in Geophysics*, *17*(2), 113–122. <https://doi.org/10.5194/npg-17-113-2010>. Retrieved from <http://arxiv.org/abs/1003.0253> (arXiv: 1003.0253).
- Zhang, Y., Jeevanjee, N., & Fueglistaler, S. (2020). Linearity of outgoing longwave radiation: From an atmospheric column to global climate models. *Geophysical Research Letters*, *47*(17), e2020GL089235. <https://doi.org/10.1029/2020GL089235>
- Zhou, C., Zelinka, M. D., & Klein, S. A. (2017). Analyzing the dependence of global cloud feedback on the spatial pattern of sea surface temperature change with a Green's function approach. *Journal of Advances in Modeling Earth Systems*, *9*(5), 2174–2189. <https://doi.org/10.1002/2017MS001096>
- Zhu, J., Poulsen, C. J., & Tierney, J. E. (2019). Simulation of Eocene extreme warmth and high climate sensitivity through cloud feedbacks. *Science Advances*, *5*(9), eaax1874. <https://doi.org/10.1126/sciadv.aax1874>